

Telescope Array Bursts, Radio Pulses and Axion Quark Nuggets

Xunyu Liang and Ariel Zhitnitsky

Department of Physics and Astronomy, University of British Columbia, Vancouver, V6T 1Z1, BC, Canada

Telescope Array (TA) experiment has recorded [1, 2] several short time bursts of air shower like events. These bursts are very distinct from conventional single showers, and are found to be strongly correlated with lightnings. In our previous work [3] we proposed that these bursts represent the direct manifestation of the dark matter annihilation events within the so-called axion quark nugget (AQN) model. In the present work we suggest to test this proposal to search for the radio signals in frequency band $\nu \in (0.5 - 200)$ MHz which must be synchronized with the TA bursts.

I. INTRODUCTION

This work is tightly linked to our recent proposal [3] interpreting the mysterious bursts observed by Telescope Array (TA) experiment [1, 2] in terms of the AQN annihilation events under the thunderstorm. These events are very unusual and cannot be interpreted in terms of conventional single showers as reviewed below. In the present work we shall argue that the proposed mechanism [3] in terms of the AQN annihilation events inevitably predict the radio wave pulses which must be synchronized with TA bursts. Based on this prediction we suggest to test our proposal by searching for the radio signals in frequency band $\nu \in (0.5 - 200)$ MHz which must be synchronized with the TA bursts.

Such test would unambiguously support or refute the proposal because the main arguments of the present work based on synchronization which represents pure geometrical property of the system. This is because the radio pulse and the TA burst are originated from the same location, emitted at the same instant, and propagate with the speed of light. This feature of synchronization is not sensitive to many assumptions and uncertainties which were inevitably present in estimates [3] interpreting the TA bursts as the AQN annihilation events.

Our presentation is organized as follows. In next section II we overview the TA bursts observations [1, 2] and the basic ideas of the proposal [3] with the resolution of these puzzling bursts in terms of the AQN annihilation events. In sections III and IV we argue that the emission of the radio pulse is inevitable consequence of the proposed mechanism, and we estimate its numerical characteristics. In sections V and VI we estimate the radio pulse due to the Earth's magnetic field. Finally, section VII is our conclusion where we suggest to search for a synchronized radio pulse with TA burst.

II. TA BURSTS AS THE AQN ANNIHILATION EVENTS UNDER THUNDERCLOUDS

The main goal of this section is to overview the basic idea of the proposal [3]. We organize this section as follows: first, in subsection II A we overview the TA bursts observations [1, 2] emphasizing on the very distinct features of the events. In subsection II C we explain the

resolution of these puzzling bursts in terms of the AQN annihilation events. In subsection II B we highlight the very few key elements of the AQN construction relevant for this work by referring to original paper [3] for all less important elements of the proposal. In other words, in the subsection II B we shall only mention the crucial ingredients related to the physics of emission of the radio pulses, which represent the topic of the present work. Such organization of this work helps us to avoid an unavoidable repetition of the background material which can be found in [3].

A. Mysterious bursts observed by [1, 2]

The unusual features of the bursts recorded by [1, 2] can be briefly formulated as follows:

1. All reconstructed air shower fronts for the burst events are much more curved than usual cosmic ray (CR) air showers. This feature is expressed in terms of the time- spreading versus spatial-spreading of the particles in the bursts. The corresponding “curvature” is much more pronounced for the bursts in comparison with conventional CR air showers, see see Fig. 3 and Fig. 4 in [1]. Furthermore, the bursts events do not have sharp edges in waveforms in comparison with conventional CR events;

2. The events are temporally clustered within 1 ms, which would be a highly unlikely occurrence for three consecutive conventional HE CR hits in the same area within a radius of approximately 1 km. The total 10 burst events have been observed during 5 years of observations. The authors of ref. [1] estimate the expectation of chance coincidence is less than 10^{-4} for five years of observations. If one tries to fit the observed bursts with conventional code, the energy for HE CR events should be in 10^{13} eV energy range, while the observed bursts correspond to $(10^{18} - 10^{19})$ eV energy range as estimated by signal amplitude and distribution. Therefore, the estimated energy from individual events within the bursts is five to six orders of magnitude higher than the energy estimated by event rate.

3. Most of the observed bursts are “synchronized” (difference between burst and lightning is less than 1 ms) or “related” (difference between burst and lightning is less than 200 ms) with the lightning events. Some of

them bursts are not related to any lightnings. However, all 10 recorded bursts occur under thunderstorm.

It is very hard to understand all these features in terms of conventional CR physics as the bursts cannot be reconciled with conventional CR physics. At the same time all unusual features (including the energetics, the flux estimates, the time and spatial spreading of each events within the bursts) as listed in items **1-3** above can be naturally explained within the AQN framework. Before we proceed with corresponding explanation we have to briefly overview the basic features of the AQN model to explain the nature and the source of the TA bursts. This is the topic of the next subsection **II B**.

B. The AQNs under the thunderclouds

The axion quark nugget (AQN) dark matter model [4] was invented long ago with a single motivation to naturally explain the observed similarity between the dark matter and the visible densities in the Universe, i.e. $\Omega_{\text{DM}} \sim \Omega_{\text{visible}}$ without any fitting parameters. The AQN construction in many respects is similar to the Witten's quark nuggets, see [5–7], and review [8]. This type of DM is “cosmologically dark” not because of the weakness of the AQN interactions, but due to their small cross-section-to-mass ratio, which scales down many observable consequences of an otherwise strongly-interacting DM candidate.

There are two additional elements in the AQN model compared to the original models [5–8]. First new element is the presence of the axion domain walls which are copiously produced during the QCD transition¹. This domain wall plays a dual role: first it serves as an additional stabilization factor for the nuggets, which helps to alleviate a number of problems with the original nugget construction [5–8]. Secondly, the same axion field $\theta(x)$ generates the strong and coherent \mathcal{CP} violation in the entire visible Universe.

Another feature of the AQN model which plays absolutely crucial role for the present work is that nuggets can be made of *matter* as well as *antimatter* during the QCD transition. Precisely the coherence of the \mathcal{CP} violating field on large scale mentioned above provides a preferential production of one species of nuggets made of *antimatter* over another species made of *matter*. The preference is determined by the initial sign of the θ field when the formation of the AQN nuggets starts. The direct consequence of this feature along with coherent \mathcal{CP}

violation in entire Universe is that the DM density, Ω_{DM} , and the visible density, Ω_{visible} , will automatically assume the same order of magnitude densities $\Omega_{\text{DM}} \sim \Omega_{\text{visible}}$ without any fine tuning. We refer to the original papers [25–28] devoted to the specific questions related to the nugget's formation, generation of the baryon asymmetry, and survival pattern of the nuggets during the evolution in early Universe with its unfriendly environment, see also independent analysis [29] confirming these basic results.

Precisely the AQNs made of antimatter are capable to release a significant amount of energy when they enter the Earth's atmosphere and annihilation processes start to occur between antimatter hidden in form of the AQNs and the atmospheric material. The emission of positrons from the nuggets made of antimatter during the thunderstorms plays the crucial role in the proposal [3]. This is because the thunderclouds are characterized by large preexisting electric field \mathcal{E} which serves as a trigger and accelerator of the liberated positrons.

We refer to review papers [30, 31] devoted to study of the lightning where pre-existing electric field \mathcal{E} plays a crucial role in dynamics of the lightning processes. While there is a consensus on typical parameters of the electric field which are important for the lightning dynamics, the physics of the of the initial moment of lightning remains a matter of debate, and refs [30, 31] represent different views on this matter, see also references [32–34] where some specific elements of existing disagreement have been explicitly formulated and debated.

For our purposes, however, the disputable elements do not play any role in our studies. Important elements for the present work, which are not controversial, are the temporal and spatial characteristics of the electric field \mathcal{E} and their values under thunderclouds. These parameters are well established and are not part of the debates, and we quote these parameters below. The electric field \mathcal{E} in the thunderclouds is characterized by the following parameters [30, 31]

$$\mathcal{E} \simeq \frac{\text{kV}}{\text{cm}}, \quad l_a \simeq 100 \text{ m}, \quad \tau_{\mathcal{E}} \simeq \frac{l_a}{c} \simeq 0.3 \mu\text{s} \quad (1)$$

where l_a is the so-called avalanche length.

If the AQN enters the electric field (1) along its path it may liberate the positrons from AQNs as the additional energy ΔE assumes the same order of magnitude as the binding energy $E_{\text{bound}} \sim \text{keV}$ of the positrons, i.e.

$$\Delta E \simeq [e\mathcal{E} \cdot R_{\text{cap}}] \sim 2 \text{ keV} \gtrsim E_{\text{bound}}. \quad (2)$$

In this formula R_{cap} is a typical distance (from the nugget's core) where positrons reside. These excited positrons localized sufficiently far away from the nugget's core due to the large rate of elastic collisions with air molecules which kick them off from the unperturbed ground state positions. The R_{cap} which enters (2) can be estimated in terms of the ionization charge Q and internal temperature of the nuggets $T \simeq 10 \text{ keV}$,

$$R_{\text{cap}} \simeq \frac{\alpha Q}{T} \sim 2 \text{ cm}, \quad (3)$$

¹ The axion field had been introduced into the theory to resolve the so-called the strong \mathcal{CP} problem which is related to the fundamental initial parameter $\theta_0 \neq 0$. This source of \mathcal{CP} violation is no longer available at the present time as a result of the axion's dynamics in early Universe. One should mention that the axion remains the most compelling resolution of the strong \mathcal{CP} problem, see original papers on the axion [9–15], and recent reviews [16–24].

see [3] with proper estimates. This additional energy (2) of order of several keV could liberate the weakly coupled positrons from the nuggets. These liberated positrons find themselves in the background of strong electric field characterized by typical length scale $l_a \simeq 100$ m according to (1). This pre-existing field will accelerate them to MeV energies on length scale (1). Indeed,

$$E_{\text{exit}} \simeq [e\mathcal{E} \cdot l_a] \sim 10 \text{ MeV} \quad (4)$$

after the positrons exit the region of strongly fluctuating electric field which is known to be present under thunderclouds.

C. “Mysterious bursts” proposal [3] confronts the observations [1, 2]

The goal of this subsection is to explain the puzzling bursts within AQN framework as proposed in [3]. It will be briefly explained how the unusual features **1-3** listed above in subsection II A can be naturally understood within the AQN framework.

1. “curvature” puzzle

We start our discussions with item **1** from the list. In the AQN framework this “curved” feature can be easily understood by noticing that essential parameter in this proposal is the initial spread of the particles determined by angle $\Delta\alpha \simeq (v_{\perp}/c) \in (0 - 0.1)$. As a result of this spread the typical time scale is determined by $\Delta\alpha$ and it could naturally assume relatively large values up to $(7 - 8) \mu\text{s}$ as estimated in (6) and consistent with observations, see Fig. 3 and Fig. 4 in [1].

Indeed, all released positrons will obviously move in the same direction which is entirely determined by the direction of the electric field \mathcal{E} at the moment of exit. Small angle $\Delta\alpha \simeq (v_{\perp}/c) \in (0 - 0.1)$ in the velocity distribution at the exit point is determined by initial energy (2) which itself is determined by transverse component perpendicular to electric field, $v_{\perp} \simeq \sqrt{2\Delta E/m} \simeq 0.1c$.

Therefore, after travelling the distance r the spatially spread range Δs is estimated as

$$\Delta s \simeq r \left(\frac{\Delta\alpha}{\cos\alpha} \right) \simeq \frac{1 \text{ km}}{\cos\alpha} \left(\frac{r}{10 \text{ km}} \right) \left(\frac{\Delta\alpha}{0.1} \right), \quad (5)$$

see Fig. 1 for precise definitions of the parameters.

At the same time, the parameter Δt can be estimated as follows:

$$\Delta t \simeq \frac{\Delta r}{c} \simeq 3 \mu\text{s} \cdot (\tan\alpha) \cdot \left(\frac{r}{10 \text{ km}} \right) \left(\frac{\Delta\alpha}{0.1} \right) \quad (6)$$

where $\Delta r \simeq r \tan\alpha \Delta\alpha$ see Fig. 1. One can infer from (6) that time spread $(2\Delta t)$ indeed could be relatively large, up to $(7 - 8) \mu\text{s}$, in contrast with conventional CR air shower when this timing spread is always below $2 \mu\text{s}$, see

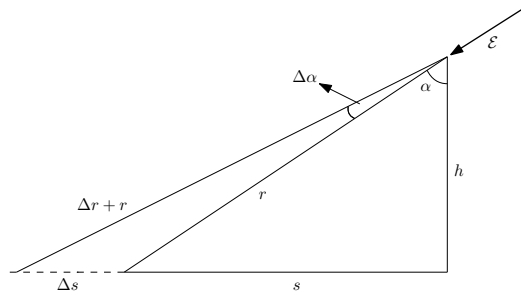


FIG. 1. The positrons move along the cone with angle $\Delta\alpha$ and inclination angle α with respect to the vertical direction. The angular spread $\Delta\alpha \ll \alpha$ is assumed to be small. The spatial spread on the surface is determined by Δs , while the additional travelling path is determined by Δr , see estimates in the text. The altitude is assumed to be within conventional range $h \simeq (4 - 12)$ km. Instant direction of the electric field \mathcal{E} at the moment of exit of the positrons is also shown.

Fig. 5 in [1]. We use $(2\Delta t)$ in our estimates with extra factor 2 as the angle $\Delta\alpha = (v_{\perp}/c)$ determining the particle distribution, could assume the positive or negative value, depending on sign of v_{\perp} with respect to instant direction of the electric field \mathcal{E} as shown on Fig. 1.

Another distinct characteristic of the the AQN framework is much stronger localization of the particles around the axis when it is typically below 2 km, see Fig. 3 and Fig. 4 in [1], in contrast with conventional CR air shower when it normally assumes much greater values around 3.5 km, Fig. 5 in [1]. This feature also finds its natural explanation within AQN framework. Indeed, the spread of the particles on the plane determined by Δs , while the timing is characterized by $\Delta t \simeq \Delta r/c$ estimated above (6). These parameters are linearly proportional to each other and assume proper values consistent with observations. Indeed,

$$\Delta r \simeq \Delta s \sin\alpha, \quad \Delta\alpha \simeq \left(\frac{v_{\perp}}{c} \right) \in (0 - 0.1) \quad (7)$$

such that $2\Delta t$ may vary between $(0.5 - 8) \mu\text{s}$ when $2\Delta s$ changes between $(0.5 - 2)$ km with approximately linear slope determined by electric field direction $\sin\alpha$. This behaviour² is consistent with observed events presented on Fig. 3 and Fig. 4 in [1].

This behaviour in terms of the timing and spatial spreads for the bursts should be contrasted with conventional CR distribution when the timing spread is much shorter and always below $2 \mu\text{s}$ while the spatial spread

² One should comment here that the actual trajectories of the positrons are not the straight lines due to the Earth’s magnetic field $\mathcal{B} \sim 0.5$ Gauss as we discuss in section V. However, the main point here is that the emitted positrons are characterized by the same velocity and localization at the instant of exit. Therefore the presence of the magnetic field \mathcal{B} does not spoil our estimates for the temporal and spatial spreads given by (7) which must hold irrespectively to the presence of \mathcal{B} .

is much longer, up to 3.5 km, see Fig. 5 in [1]. This difference between the distributions in bursts and conventional CR air showers was coined as the “curvature” puzzle. As we mentioned above, this puzzle is naturally resolved within the AQN framework.

Similar arguments also explain why the observed events do not have sharp edges in waveforms (see Fig. 6 in [1]). The point is that conventional CR air showers typically have a single ultra-relativistic particle which generates a very sharp edge in waveforms. It should be contrasted with large number of positrons which produce the non-sharp edges in waveforms in the AQN-based proposal.

What is important here is that these features are not sensitive to many uncertainties which inevitably present in estimates of [3]. This is because the “curvature” feature discussed above has pure kinematical (geometrical) nature. It is not related to any complicated problems such as a large Mach number, turbulence, the AQN internal structure, the dynamics of the electric field under the thunderstorm, etc. One can say that the “curvature” property observed in bursts is an almost model-independent consequence of the AQN framework, not sensitive to many uncertainties of the absolute normalization factors in the estimates presented in [3]. The same comment also applies to the property of the non-sharp edges in waveforms as this feature is also very generic consequence of the AQN framework, not related to any uncertainties in the estimates [3].

2. “clustering” puzzle

The item 2 shows a dramatic inconsistency (when interpreted in terms of the CR air showers) for the bursts events when the event rate suggests that the energy should be in 10^{13} eV range, while the intensity of the events suggests $(10^{18} - 10^{19})$ eV range. In the AQN framework the burst represents the *cluster* of events related to one and the same AQN which traverses the distance $L_{\text{burst}} \simeq 0.25$ km during $\Delta t = 1$ ms. In different words, the burst is not a collection of independent events. Conventional Poissonian distribution does not apply here. Instead, the bursts represent the clustering events when the intensities are determined by the numbers of liberated positrons when the AQNs enter strong electric field under the thunderstorm. Furthermore, the spatial spread for each individual event within the same cluster also lies within the same range ~ 1 km according to (5). On the one hand, the observations are extremely hard to explain in terms of conventional CR air showers. On the other hand, the same observations are perfectly consistent with the AQN based estimates.

3. “synchronization” puzzle

According to item 3 most of the observed bursts are “synchronized” or “related” to the lightning events. However, some of the bursts are not related to any lightnings. Therefore, one cannot assume that the bursts are initiated by the lightning events. However, all 10 recorded bursts occur under thunderstorm. This is very puzzling property of the bursts if interpreted in terms of the conventional CR air showers because it is very hard to understand how the thunderstorms may dramatically modify CR features as discussed above.

At the same time the “synchronization” puzzle is perfectly consistent with AQN based proposal [3] because the thunderstorm with its pre-existing electric field (1) plays a crucial role in the mechanism as the electric field instantaneously liberates the positrons and also accelerates them up to 10 MeV energies. The mean free path of such energetic positrons is sufficiently long such that these positrons can easily reach the TA surface detectors, and can produce the signals consistent with the bursts.

To summarize this section: the mysterious bursts (with highly unusual features as listed by items 1-3 in Section II A) of shower-like events observed by T ASD [1, 2] are naturally interpreted as the cluster events generated by the AQNs propagating in thunderstorm environment. Some of the features of these events (such as intensity and the basic normalization factors) suffer inevitable uncertainties due to very complex dynamical properties of the system (the AQN propagation under thunderstorm with large Mach number). However, there are some features of the system such as given by eqs. (5), (6), (7) which are not sensitive to these uncertainties and represent almost model-independent consequences of the proposal [3].

III. RADIO PULSE AND TA BURST AS SYNCHRONIZED EVENTS

This section is devoted to studies of the radio signals which always accompany TA bursts when interpreted in terms of the AQN annihilation events under the thunderstorm as presented in previous section II. We shall argue below that the emission of the radio pulse is inevitable consequence of the proposed mechanism. Furthermore, the radio pulse must be synchronized with TA burst irrespectively whether the bursts are related or unrelated to the lightning events. This synchronization must be within $10 \mu\text{s}$ from every TA event as the positrons and radio waves originated from the same location at the same instant and both propagate with the speed of light. As the typical time and spatial spreads of the TA events do not exceed $10 \mu\text{s}$ the synchronization must be within the same temporal and spatial range.

This section is organized as follows. In next subsection III A we study the trajectory of the liberated positrons in a typical electric field characterized by parameters (1). We analyze the total intensity and the angular distribu-

tion of the radio emission in subsection III B, while the spectral properties of the pulse are studied in subsection III C. Finally, in subsection III D we study the properties of the electric field's pulse which can be detected at the surface detector area.

A. Positron's acceleration in electric field under thunderstorm

Our goal here is to describe the dynamics of the liberated positrons which are emitted with initial energies in keV range according to (2). To simplify things we assume that the electric field \mathcal{E} directed along \mathbf{z} -axis is uniform and characterized by parameters (1). In this case the solution is well known [35] and can be described as follows. At the very initial moment of acceleration at $t \ll t_0$ the particle moves with non-relativistic velocities according to conventional formulae:

$$\begin{aligned} z(t) &\simeq \frac{p_z^0}{m}t + \frac{|e|\mathcal{E}}{2m}t^2, & t \ll t_0 \equiv \frac{mc}{|e|\mathcal{E}} \\ x_{\perp}(t) &\simeq \frac{p_{\perp}^0}{m}t, & \frac{p_{\perp}^0}{m} \simeq \frac{p_z^0}{m} \simeq \frac{v_{\perp}}{c}, \end{aligned} \quad (8)$$

where $p_z^0 \sim p_{\perp}^0$ is the initial positron's momentum at the moment of liberation from AQN. Numerically, this non-relativistic portion of the positron's journey is very short as $t_0 \sim 10^{-8}$ s. It will be ignored in all our discussions which follow.

The portion of the positron's journey which plays the key role in our discussions is the motion with constant acceleration $e\mathcal{E}/m$ and the velocity close to c . The corresponding motion is determined by the formulae:

$$\begin{aligned} z(t) &= \frac{c}{|e|\mathcal{E}} \left[\sqrt{(p_{\perp}^0)^2 + m^2c^2 + (p_z^0 + |e|\mathcal{E}t)^2} - \frac{E^0}{c} \right], \\ x_{\perp}(t) &\simeq \frac{cp_{\perp}^0}{|e|\mathcal{E}} \ln \frac{2|e|\mathcal{E}t}{mc}, & t \gg t_0 \equiv \frac{mc}{|e|\mathcal{E}} \end{aligned} \quad (9)$$

where $E^0 \simeq (mc^2 + \Delta E)$ is the total initial energy of positrons at the moment of liberation.

The most important observation here is that the positrons move with ultra-relativistic velocities for most of the time, and the displacement in transverse direction (with respect to the orientation of the electric field) is very modest such that the majority of the particles remain in the system and continue their acceleration for the entire time interval $\tau_{\mathcal{E}} \sim 0.3 \mu\text{s}$ determined by parameter l_a according to (1). At this point most of the particles assume very high energy close to 10 MeV according to (4) while transverse momentum distribution is characterized by $(v_{\perp}/c) \lesssim 0.1$. The elastic scattering of the positrons off the atmospheric molecules during this short journey plays very minor role as the kinetic energy of positrons being in keV range at the initial instant assumes MeV energies very quickly such that the corresponding cross section never becomes sufficiently large to modify the positron's dynamics as computed above in vacuum.

B. Intensity and the angular distribution

Our next task is to present conventional formulae for the intensity and the angular distribution of the radio emission due to the relativistic positrons (9) accelerating in electric field \mathcal{E} with parameters (1). As we discussed above the velocity \mathbf{v} of the positrons is mostly oriented along the electric field while v_{\perp} is small. Therefore, we assume that $\mathcal{E} \parallel \mathbf{v}$ to simplify our formulae which follow. In this simplified geometry the angular distribution for the intensity assumes the following form, see e.g. [35, 36]:

$$\frac{dI(t)}{d\Omega} \simeq \frac{N^2 e^2 \mathbf{a}^2(t)}{4\pi c^3} \frac{\sin^2 \theta}{(1 - \frac{v}{c} \cos \theta)^5}, \quad \mathbf{a} \equiv \frac{e\mathcal{E}}{m\gamma^3}, \quad (10)$$

where N is the number of coherent positrons participating in the radio wave emission, to be estimated below. The angle θ in this expression is defined as usual as the angle between the velocity \mathbf{v} of the charged particle at the moment of emission and the direction \mathbf{n} of the observer, i.e. $\mathbf{v} \cdot \mathbf{n} = v \cos \theta$. Formula (10) explicitly shows that the emission mostly occurs along \mathcal{E} direction as $\mathcal{E} \parallel \mathbf{v}$. This is precisely the same direction where burst events are recorded as shown on Fig. 1.

Integration over all angles leads to well known expression for the total intensity:

$$I(t) \simeq \frac{2N^2 e^2}{3c^3} [\mathbf{a}^2(t)\gamma^6], \quad \gamma \equiv \frac{1}{\sqrt{1 - \frac{v^2}{c^2}}} \quad (11)$$

Formula (11) represents the well known feature of the emission that the intensity is strongly enhanced for ultra-relativistic particles, which is obviously the case for positrons accelerated up to 10 MeV energies according to (4). This implies that the relativistic enhancement factor entering (11) is enormous: $(E_{\text{exit}}/m)^6 \sim 10^8$.

C. Spectral characteristics of the radio emission

The main goal of this subsection is to understand the spectral characteristics of the radio emission. It will also allow to estimate the coherence factor N entering (10) and (11) as this factor obviously depends on the frequency of radiation and corresponding wave length.

The starting point for these studies is spectral property of the electric field \mathbf{E}_{ω} emitted by the accelerating positrons, see e.g. [35, 36]:

$$\mathbf{E}_{\omega} = \int_{-\infty}^{+\infty} \mathbf{E} e^{i\omega t} dt, \quad \mathbf{E} = \frac{Ne \mathbf{n} \times ((\mathbf{n} - \frac{\mathbf{v}}{c}) \times \mathbf{a})}{c^2 R (1 - \frac{\mathbf{n} \cdot \mathbf{v}}{c})^3}, \quad (12)$$

where all quantities at the right hand side of eq. (12) must be computed as the retarded times t' :

$$t' \approx t - \frac{R_0}{c} + \frac{\mathbf{n} \cdot \mathbf{v} t'}{c} \rightarrow t = t' \left(1 - \frac{\mathbf{n} \cdot \mathbf{v}}{c} \right) + \frac{R_0}{c} \quad (13)$$

where we assumed that the positrons move with approximately constant time-independent velocity $|\mathbf{v}| \approx c$. This

assumption allows us to represent the Fourier component \mathbf{E}_ω in the following form

$$\mathbf{E}_\omega = \frac{e^{ikR_0}}{R_0} \left(\frac{Ne}{c^2} \right) \left(\frac{\omega}{\omega'} \right)^2 \left[\mathbf{n} \times \left(\left(\mathbf{n} - \frac{\mathbf{v}}{c} \right) \times \mathbf{a}_{\omega'} \right) \right], \quad (14)$$

where ω' and $\mathbf{a}_{\omega'}$ are defined as follows

$$\omega' \equiv \omega \left(1 - \frac{\mathbf{n} \cdot \mathbf{v}}{c} \right), \quad \mathbf{a}_{\omega'} = \int_{-\infty}^{+\infty} \mathbf{a}(\mathbf{t}') e^{i\omega' t'} dt' \quad (15)$$

which precisely the combination entering the Fourier transform (12).

Using Fourier component for \mathbf{E}_ω as given by (14) and magnetic component $\mathbf{B}_\omega = i(\mathbf{k}_\omega \times \mathbf{E}_\omega)$ one can compute the energy $dE_{\mathbf{n}\omega}$ emitted into solid angle $d\Omega$ with frequency interval $d\omega$ [35, 36]:

$$\frac{dE_{\mathbf{n}\omega}}{d\Omega d\omega} = \left(\frac{N^2 e^2}{4\pi^2 c^3} \right) \left(\frac{\omega}{\omega'} \right)^4 \left| \mathbf{n} \times \left(\left(\mathbf{n} - \frac{\mathbf{v}}{c} \right) \times \mathbf{a}_{\omega'} \right) \right|^2. \quad (16)$$

One can simplify this expression by assuming that the $\mathbf{a} \parallel \mathbf{v}$ as we previously discussed. Furthermore, one can carry out the integration over $d\Omega$ by integrating over $d\omega'$ for a given ω as these two variables are related according to (15). Indeed, the emission is mostly concentrated along the cone with $\theta^2 \approx (1 - v^2/c^2)$. Furthermore,

$$\omega' \equiv \omega \left(1 - \frac{\mathbf{n} \cdot \mathbf{v}}{c} \right) \approx \frac{\omega}{2} \left[\frac{1}{\gamma^2} + \theta^2 \right], \quad (17)$$

where we expanded $\cos \theta \approx (1 - \theta^2/2)$ and represented small factor $(1 - v/c) \approx 1/(2\gamma^2)$ in terms of the conventional combination γ which is valid approximation for ultra-relativistic positrons with $|\mathbf{v}| \simeq c$. Now, integration over angles $d\Omega$ can be replaced by integration over $d\omega'$ as these two variables are related (17). Therefore,

$$d\Omega = 2\pi \sin \theta d\theta \approx 2\pi \left(\frac{d\theta^2}{2} \right) \approx 2\pi \left(\frac{d\omega'}{\omega} \right) \quad (18)$$

such that the energy dE_ω emitted within the frequency interval $d\omega$ assumes the form

$$\frac{dE_\omega}{d\omega} = \left(\frac{N^2 e^2 \omega^2}{2\pi c^3} \right) \int_{\frac{\omega}{2\gamma^2}}^{\infty} \frac{d\omega' |\mathbf{a}_{\omega'}|^2}{(\omega')^3} \left[2 - \frac{\omega}{\omega' \gamma^2} \right], \quad (19)$$

where the low limit of integration is determined by $\theta = 0$ in Eq. (17).

The same expression can be thought as the angular distribution of the emission

$$\frac{dE_\omega}{d\omega} = \left(\frac{N^2 e^2 \gamma^6}{2\pi c^3} \right) \frac{16 |\mathbf{a}_{\omega'}|^2}{(1 + \gamma^2 \theta^2)^3} \left[\frac{\gamma^2 \theta^2}{1 + \gamma^2 \theta^2} \right] \cdot \frac{d\Omega}{2\pi}, \quad (20)$$

where $|\mathbf{a}_{\omega'}|$ should be expressed in terms of θ according to (17).

Our next task is to model the acceleration $\mathbf{a}(t)$ for a typical thunderstorm electric field with parameters (1). The corresponding Fourier transform (15) determines $\mathbf{a}_{\omega'}$

which enters expression for $dE_\omega/d\omega$ as given by (19). Our simplest possible choice is as follows:

$$\mathbf{a}(t) \approx \frac{e\mathcal{E}}{\gamma^3 m}, \quad t \in (0, \tau_\mathcal{E}), \quad (21)$$

while $\mathbf{a}(t) \approx 0$ for t being outside of this interval. The corresponding expression for $\mathbf{a}_{\omega'}$ defined by (15) assumes the form

$$|\mathbf{a}_{\omega'}|^2 = \frac{4e^2 \mathcal{E}^2}{m^2 \gamma^6 \omega'^2} \sin^2 \left(\frac{\omega' \tau_\mathcal{E}}{2} \right). \quad (22)$$

Now we can perform the integration $d\omega'$ in (19). For our simple model for acceleration (21) the integral can be approximately computed for small $(\omega' \tau_\mathcal{E}) \ll 1$. This leads us to the order of magnitude estimate for $dE_\omega/d\omega$:

$$\frac{dE_\omega}{d\omega} \approx \left(\frac{N^2 e^2}{2\pi c^3} \right) \cdot \left(\frac{e^2 \mathcal{E}^2 \tau_\mathcal{E}^2}{m^2 \gamma^6} \right) \cdot \left(\frac{4\gamma^4}{3} \right). \quad (23)$$

The same expression can be derived from (20) by integrating over the angles $d\Omega$.

This spectral density holds as long as ω is sufficiently small. To be more precise:

$$\omega \lesssim \gamma^2 \tau_\mathcal{E}^{-1}, \quad (24)$$

which represents the dominant contribution to the integral (19) for small ω . The emission with higher frequencies will be power-suppressed as ω^{-2} .

Few comments are in order. The spectral density (23) integrated over all angles $d\Omega$ approximately constant and does not depend on ω as long as condition (24) is satisfied. This is of course a well-known feature of the constant acceleration (21) which we used as a simplified model for the electric field. In reality, the electric field under thunderstorm obviously fluctuates in time and space. This will obviously modify the spectral features (23). However, we expect that a typical frequency of the emission as given by (24) will hold because it is basically determined by the typical time scale of the problem $\tau_\mathcal{E}$ and expected relativistic factor γ which is not very sensitive to the details of the fluctuating electric field \mathcal{E} .

The crucial observation here is that the typical frequency of emission is not simply given by the scale $\tau_\mathcal{E}^{-1}$ as one could naively expect based on dimensional arguments. Rather, the emission extends to much broader region due to the large relativistic factor γ^2 as eq. (24) states.

We postpone for the detail numerical estimates to section IV. Now we want to make few simple numerical estimates supporting the main claim of this work that the frequency of emission is in the radio band $\nu \in (0.5 - 200)$ MHz. Furthermore, the emission is mostly oriented along the same direction where TA bursts are recorded. Therefore, one should anticipate a strong synchronization between the TA bursts and the radio pulses as both emission occurs at the same location at the same instant, and propagate to the corresponding detectors with the same speed of light. These features are not very sensitive to

details of the dynamics of the AQNs, nor specific features of electric field under thunderstorm. Rather, all these features are inevitable consequences of the basic AQN framework along with pure geometrical properties of these observables.

With these comments in mind we can represent the typical band as follows

$$\nu \lesssim \frac{\gamma^2}{2\pi\tau_{\mathcal{E}}} \approx 200 \text{ MHz}, \quad \nu \equiv \frac{\omega}{2\pi}, \quad \gamma \approx 20, \quad (25)$$

which we expect to hold irrespectively to specific features of the AQN model as it is entirely determined by well established typical time scales of the electric field under the thunderstorm (1). One could naively think that the typical frequency of emission could be extrapolated to very low ν as the spectral density (23) apparently does not depend on frequency. This is not quite correct conclusion though as we shall discuss in next section IV.

D. Radio pulse of the electric field

The goal of this section is to estimate the intensity of the electric field (12) at very large distances R where it can be potentially detected. The orientation of \mathbf{E} field is determined by cross product (12) where one can assume (for the simplicity of the numerical estimates) that $\mathbf{v} \parallel \mathbf{a}$, similar to our previous estimates for the spectral intensity of the emission (19). The absolute value for $|\mathbf{E}|$ at large distances can be estimated as follows

$$|\mathbf{E}| \approx \frac{Ne|\mathbf{a}|\theta}{c^2R} \left(\frac{\omega}{\omega'}\right)^3 \approx \frac{Ne|\mathbf{a}|\theta}{c^2R} \left(\frac{2\gamma^2}{1+\gamma^2\theta^2}\right)^3, \quad (26)$$

where R is the distance from the emission site to the area where the electric field $|\mathbf{E}|$ could be recorded. It should not be confused with parameter r which enters all formulae from section II C and describes the distance from the emission site to the SD site where the energetic positrons could be detected. Numerically these parameters are similar, of course. However, the radio signal can be observed in a different location from the local area where the positrons hit the T ASD.

This formula explicitly shows that the time duration of the radio pulse and its properties are unambiguously determined by the features of the electric field \mathcal{E} under thunderstorm. For simple model (21) this implies that the radio pulse lasts $\tau_{\mathcal{E}}$ while the absolute value of the pulse is estimated as

$$|\mathbf{E}(\theta, t)| \approx \frac{Ne\theta}{c^2R} \left(\frac{2\gamma^2}{1+\gamma^2\theta^2}\right)^3 \left(\frac{e\mathcal{E}(t)}{m\gamma^3}\right), \quad t \in (0, \tau_{\mathcal{E}}). \quad (27)$$

It is important to emphasize that the duration of the pulse $\tau_{\mathcal{E}}$ is not very sensitive to the details of the AQN model as it is entirely determined by well established typical time scales of the electric field under the thunderstorm (1). This feature is very similar to our previous arguments regarding a typical frequency of the radio

emission (25). At the same time the intensity of the pulse is highly sensitive to the details of the AQN model as it depends on the number of positrons N participating in the emission. In this respect this feature of insensitivity to any specific details of the AQN model for the pulse duration $\tau_{\mathcal{E}}$ and the frequency ν as given by (25) is similar to our studies of the TA burst events when such features as the ‘‘curvature’’, the timing and the spatial spread of the bursts are not sensitive to the details of the AQN model, but entire determined by the geometry as reviewed in section II C. This should be contrasted with estimations [3] of the intensity of the TA bursts which are highly sensitive to specific features of the model, which are hard to carry out in a quantitative manner.

IV. NUMERICAL ESTIMATES

Our goal here is to present some numerical results using parameters which had been used in our previous estimations [3] related to puzzling T ASD bursts as reviewed in section II C. One should emphasize from the very beginning that the corresponding estimates suffer from huge uncertainties, and should be considered as the order of magnitude estimates, at the very best. Our main arguments of the present work are not based on these highly model dependent estimates. Rather, our main arguments are based on essentially model-independent features of the radio emission such as typical frequency band (25) and strong synchronization between T ASD burst events and the radio emission. Nevertheless, we think that an order of magnitude estimates for the amplitude of the electric field as presented below could be useful as they demonstrate the consistency of the proposal. The same estimates also demonstrate the principle feasibility to detect such radio signals.

We start with numerical estimation of the strength of the electric field of the pulse (27) in conventional units (mV/m):

$$|\mathbf{E}(\theta, t)| \approx 90 \frac{\text{mV}}{\text{m}} \cdot \left[\frac{(\gamma\theta)}{(1+\gamma^2\theta^2)^3} \right] \cdot \left(\frac{\gamma}{20}\right)^2 \cdot \left(\frac{N}{10^9}\right) \cdot \left(\frac{10 \text{ km}}{R}\right), \quad t \in (0, \tau_{\mathcal{E}}) \quad (28)$$

where factor N is the number of the coherent positrons participating in the emission, to be estimated below. The orientation of the electric field is determined by the cross product as given by (12), and it is approximately (up to small angle θ) points along \mathbf{a} which represents the direction of the electric field under thundercloud at the instant of emission. The temporal shape of the pulse (bipolar, unimodal or even more complicated form) is also determined by the same fluctuating electric field \mathcal{E} at the moment of emission. The intensity of the field is strongly peaks along \mathbf{n} with typical angle $\theta\gamma \lesssim 1$, see Fig. 2 for a precise angular distribution of $|\mathbf{E}(\theta)|$.

Our next task is the estimation of parameter N entering (28). Our estimates will be entirely based on the

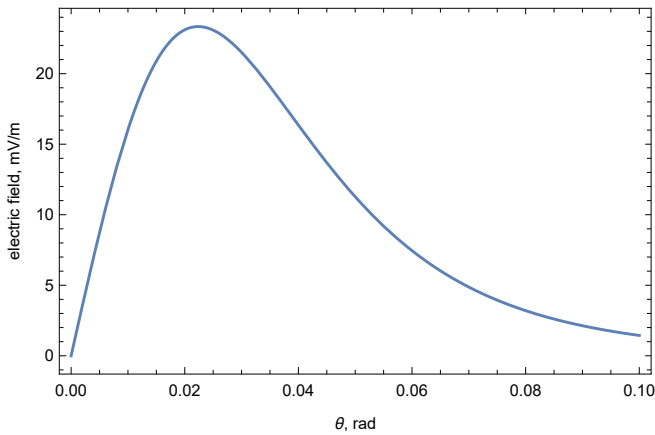


FIG. 2. Strength of electric field (28) induced under thunderstorm versus observation angle θ . The parameters are chosen to be $N = 10^9$, $\gamma = 20$, $\mathcal{E} = 1 \text{ kV/cm}$.

observations, rather than on theoretical computations which inevitably suffer from huge uncertainties as reviewed in section II C. Therefore, the logic of our estimation of parameter N is as follows. Let us assume that the TASD bursts which have been recorded are indeed due to the positrons emitted by AQNs as proposed in [3]. In this case the number of detected particles must be proportional to the density of particle detectors. This number is known for presently operating 507 SD detectors with area 3 m^2 each. These detectors are covering 680 km^2 total area. The number of detected particles must be also proportional to the area $\sim \pi(r\Delta\alpha)^2$ where particles had been recorded by TASD during a single event within the burst. Therefore, the number of positrons N at the emission site can be estimated from the following relation:

$$N_{\text{positrons}}^{\text{detected}}[\Delta s] \approx N \left[\frac{507 \cdot 3 \text{ m}^2}{680 \text{ km}^2} \right] [\langle e^{-\frac{r}{\lambda}} \rangle] [\pi(r\Delta\alpha)^2] \quad (29)$$

In our estimate (29) the number of detected particles being recorded over the surface area $\pi(\Delta s)^2$ (left hand side of eq. (29)) varies for different events within a single burst, and it normally varies in the range $(2 - 6) \cdot 10^2$. In our estimate (29) we inserted the suppression factor $\langle \exp(-r/\lambda) \rangle \sim 0.1$ introduced in [3] to account for some attenuation of the positrons travelling a distance $r \sim 10 \text{ km}$ or so when the mean free path λ for positrons with few MeV energy is order of kilometre at the sea level and several kilometres at higher altitudes. One should also note that $\pi(r\Delta\alpha)^2$ on the right hand side of eq. (29) is not identically the surface area $\sim \pi(\Delta s)^2$ where particles are being recorded. These areas are directly related to each other through angle α according to (5), see Fig. 1 for notations.

The relation (29) suggests that number N entering (28) for $(r\Delta\alpha) \sim 1 \text{ km}$ (which corresponds to a typically observed spatial spread for the burst events) can be estimated as

$$N \approx (0.3 - 1) \cdot 10^9 \quad \text{for} \quad (r\Delta\alpha) \sim 1 \text{ km}. \quad (30)$$

This estimate for N corresponds to the amplitude of the electric field (28) on the level 20 (mV/m) measured at distance $R \simeq 10 \text{ km}$ from the source of the emission within the angle range $(\theta\gamma) \lesssim 1$ where the most of the radio emission occurs.

One should comment here that such strength of the amplitude $|\mathbf{E}|$ on the level 20 (mV/m) with the duration time of the radio pulse on the scale $\sim 0.3 \mu\text{s}$ could be recorded with existing technology, see e.g. [37] where wide-band radio interferometry ($0.1\text{--}30 \text{ MHz}$) has been used to detect such short signals with amplitudes of electric field on the level 10^2 (mV/m) , which is very close to what is required for the purposes of the present work. Therefore, such signal (28) can be in principle measured if proper instruments are designed and built at the T ASD site.

Our last task in this section is establishing of the lower frequency bound for the radio emission. The spectral density (23) which is approximately a constant, naively suggests that the spectrum extends to arbitrary low frequencies. In fact, it is a premature conclusion as formula (23) was derived assuming a constant acceleration. In reality, a typical acceleration time is determined by (1) such that one should expect that $\nu \gtrsim (2\pi\tau\mathcal{E})^{-1} \approx 0.5 \text{ MHz}$. Therefore, the AQN-induced $\sim 0.3 \mu\text{s}$ pulse represents a radio emission in the bandwidth $\nu \in (0.5 - 200) \text{ MHz}$ with the amplitude of the corresponding electric field of the order $|\mathbf{E}(\theta, t)| \sim 20 \text{ (mV/m)}$ at distance $R \sim 10 \text{ km}$ as estimated above. Important feature of this spectrum is that it is very broad. Indeed, the intensity of the radiation changes by factor two or so when the frequency varies by two orders of magnitude. Another comment which follows from Fig. 3 is that the portion of the positron's energy being converted into the radio waves is very tiny as initial positrons energy can be estimated as $10N \text{ MeV}$ when N is estimated in (30). This implies that the initial energy is many orders of magnitude greater than the radio wave energy shown on Fig. 3.

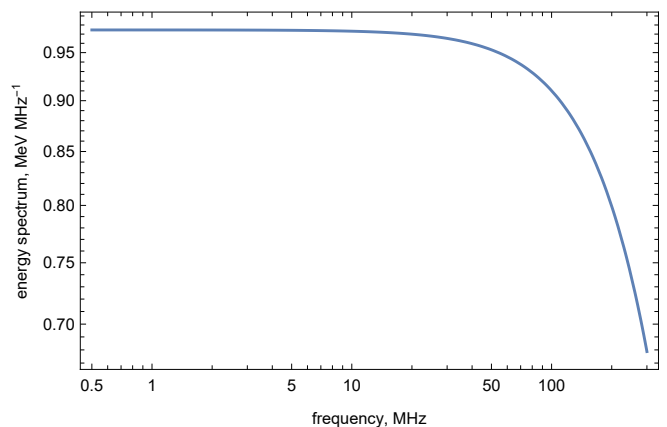


FIG. 3. Spectrum of Eq. (19) in terms of frequency ν , thunderstorm radiation. The parameters are chosen to be $N = 10^9$, $\gamma = 20$, $\mathcal{E} = 1 \text{ kV/cm}$.

The crucial point of our analysis can be formulated as

follows. This radio pulse must be synchronized with an event within TA burst within $10 \mu\text{s}$ because the TA burst and the radio emission are originated from the same location emitted at the same instant and both signals propagate with the speed of light along the same direction to be detected within $\sim \text{km}^2$ area.

It is important to emphasize that such strong synchronization must hold even if the TA bursts are not related to any lightning events and can be easily discriminated from much stronger radio emission which always accompany lightnings. Therefore, such synchronization between the radio pulses and the TA bursts, if observed, can be easily distinguished from any other possible correlation between radio emission and conventional lightning events. The correlation between flashes and radio emission during thunderstorms is well known and well documented generic feature of the the lightning discharges, see [37] with large number of references on the original literature.

V. GEOSYNCHROTRON RADIATION

Another significant radio emission is the geosynchrotron radiation which is due to presence of the Earth's magnetic field $\mathcal{B} \sim 0.5$ gauss. This effect becomes important near the end of radio emission under thunderstorm. At this instant all the positrons are ultrarelativistic ($\gamma \sim 20$) but they are no longer accelerating as they already left the region of the external electric field \mathcal{E} . Trajectory of positrons are helical in presence of the magnetic field of Earth $\mathcal{B} \sim 0.5$ gauss. The acceleration in this case is perpendicular to the direction of velocity $\mathbf{v} \perp \mathbf{a}_{\mathcal{B}}$, so it is convenient to set up the following coordinate with respect to the direction of observer \mathbf{n} :

$$\hat{\mathbf{v}} \cdot \mathbf{n} = \cos \theta, \quad \hat{\mathbf{a}}_{\mathcal{B}} \cdot \mathbf{n} = \sin \theta \cos \phi \quad (31)$$

Radius of the helical trajectory can be estimated as

$$\rho \approx \frac{c^2}{|\mathbf{a}_{\mathcal{B}}|} \approx \frac{0.7 \text{ km}}{\sin \theta_{\mathcal{B}}} \left(\frac{\gamma}{20} \right) \left(\frac{0.5 \text{ gauss}}{\mathcal{B}} \right), \quad (32)$$

$$|\mathbf{a}_{\mathcal{B}}| \approx \frac{e\mathcal{B}c \sin \theta_{\mathcal{B}}}{\gamma m},$$

where $\theta_{\mathcal{B}}$ is defined to be the angle between direction of \mathcal{B} and the velocity of positrons \mathbf{v} .

Radiation from an ultrarelativistic particle has a narrow emission angle $\theta \lesssim \gamma^{-1}$, similar to our previous discussions. However, the pulse of radiation for geosynchrotron radiation is much shorter [35, 36]:

$$\tau_{\mathcal{B}} \approx \frac{\rho}{2\gamma^3 c} = \frac{0.14 \text{ ns}}{\sin \theta_{\mathcal{B}}} \left(\frac{20}{\gamma} \right)^2 \left(\frac{0.5 \text{ gauss}}{\mathcal{B}} \right) \quad (33)$$

This interval is much shorter than the time scale $\tau_{\mathcal{E}} \sim 0.3 \mu\text{s}$ discussed previously due to extra suppression factor $\sim \gamma^{-3}$. The energy spectrum integrated over angle

$d\Omega$ is well known [35, 36, 38]:

$$\frac{dE_{\omega}}{d\omega} = \frac{c\tau_{\mathcal{B}}}{2\pi\rho} \frac{\sqrt{3}N^2 e^2}{c} \gamma \frac{\omega}{\omega_c} \int_{\omega/\omega_c}^{\infty} K_{5/3}(x) dx, \quad (34)$$

$$\omega_c = \frac{3}{2} \gamma^3 \left(\frac{c}{\rho} \right) \simeq \frac{3}{4\tau_{\mathcal{B}}},$$

where $K_{5/3}(x)$ is the modified Bessel function, and ω_c is the critical angular frequency beyond which radiation becomes negligible.

The electric field of the geosynchrotron radiation follows from (12):

$$|\mathbf{E}| = \frac{Ne|\mathbf{a}_{\mathcal{B}}|}{c^2 R} \left(\frac{\omega}{\omega'} \right)^2 \sqrt{1 - \frac{(\mathbf{n} \cdot \hat{\mathbf{a}}_{\mathcal{B}})^2}{\gamma^2}} \left(\frac{\omega}{\omega'} \right)^2$$

$$\approx \frac{Ne}{c^2 R} \left(\frac{e\mathcal{B}c \sin \theta_{\mathcal{B}}}{\gamma m} \right) \left(\frac{2\gamma^2}{1 + \gamma^2 \theta^2} \right)^2$$

$$\times \sqrt{1 - \left(\frac{2\gamma\theta \cos \phi}{1 + \gamma^2 \theta^2} \right)^2}, \quad (35)$$

The estimation of electric field strength holds as long as the positron current remains coherent. The coherent length l_{coh} can be estimated in what follows. The dispersion in velocity is $\delta v \sim v_{\perp} \lesssim 0.1c$ from Eq. (7). The condition of coherence requires the dispersion length δl to be much less than the radius ρ of trajectory:

$$\delta l \approx \frac{\delta v}{c} l_{\text{coh}} \sim \frac{v_{\perp}}{c} l_{\text{coh}} \ll \rho. \quad (36)$$

It implies $l_{\text{coh}} \sim \rho$ that is insensitive to details of local parameters such as γ and \mathcal{B} , and the geosynchrotron radiation is only significant within the first cycle of rotation.

VI. NUMERICAL ESTIMATES ON GEOSYNCHROTRON RADIATION

Similar to Sec. IV, we make numerical estimation for the electric field strength and the frequency bandwidth. Numerical estimation for the strength of the electric field of pulse (35) in conventional units (mV/m) is given as:

$$|\mathbf{E}| \approx 100 \frac{\text{mV}}{\text{m}} \cdot \frac{\sin \theta_{\mathcal{B}}}{(1 + \gamma^2 \theta^2)^2} \sqrt{1 - \left(\frac{2\gamma\theta \cos \phi}{1 + \gamma^2 \theta^2} \right)^2}$$

$$\times \left(\frac{\gamma}{10} \right)^3 \left(\frac{N}{10^9} \right) \left(\frac{10 \text{ km}}{R} \right) \left(\frac{\mathcal{B}}{0.5 \text{ gauss}} \right), \quad (37)$$

see Fig. 4 for a precise angular distribution with specific parameters. The upper limit of frequency band is determined by the critical frequency ω_c :

$$\nu \lesssim \frac{\omega_c}{2\pi} = \frac{3}{8\pi\tau_{\mathcal{B}}} \approx 600 \text{ MHz}, \quad (\theta_{\mathcal{B}} = \frac{\pi}{4}), \quad (38)$$

and the lower frequency cutoff is given by the fundamental frequency:

$$\nu \gtrsim \frac{c}{2\pi\rho} \approx 50 \text{ kHz}, \quad (\theta_{\mathcal{B}} = \frac{\pi}{4}). \quad (39)$$

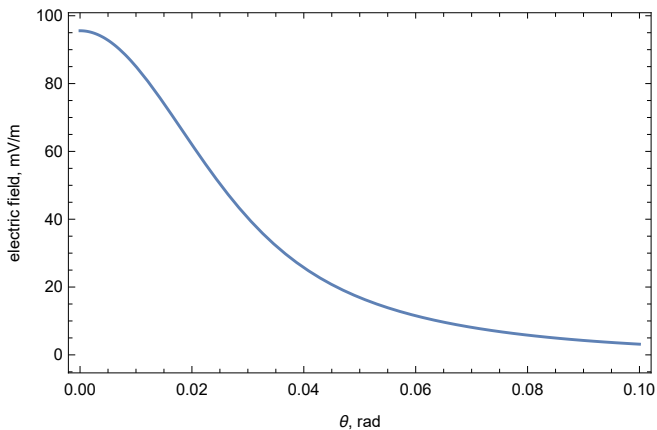


FIG. 4. Strength of electric field (35) induced by geosynchrotron radiation versus observation angle θ . The parameters are chosen to be $N = 10^9$, $\gamma = 20$, $\mathcal{B} = 0.5$ gauss, $\theta_{\mathcal{B}} = \phi = \pi/4$.

Therefore, the geosynchrotron induces a radio pulse with time duration ~ 0.14 ns in the bandwidth $\nu \in (0.05 - 600)$ MHz (see Fig. 5) and the amplitude of the corresponding electric field is of order ~ 50 mV/m at distance $R \sim 10$ km.

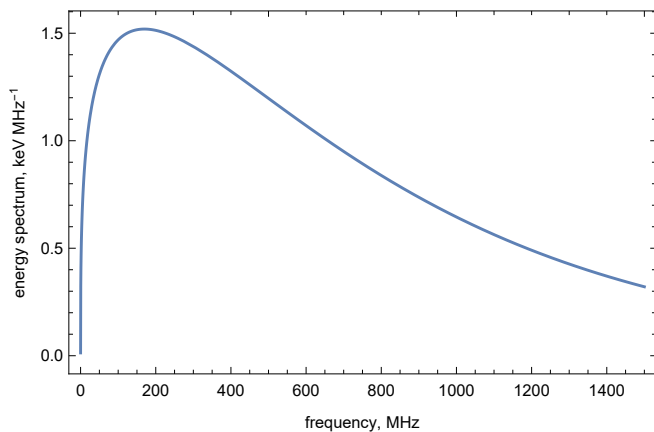


FIG. 5. Spectrum of Eq. (34) in terms of frequency ν , geosynchrotron radiation. The parameters are chosen to be $N = 10^9$, $\gamma = 20$, $\mathcal{B} = 0.5$ gauss, $\theta_{\mathcal{B}} = \pi/4$

While numerical values of the frequency bandwidth $\nu \sim (0.1 - 10^2)$ MHz and the maximal strength of electric field of the radio wave [$|\mathbf{E}| \sim (20 - 50)$ mV/m] are similar in both cases of radio pulses (which we term as \mathcal{E} -type and \mathcal{B} -type correspondingly) there is an important distinct feature, which is manifested in dramatically different time durations in these two cases. To be more precise, a \mathcal{B} -type pulse induced by geosynchrotron radiation ($\tau_{\mathcal{B}} \sim 0.14$ ns) is much shorter than \mathcal{E} -type pulse with ($\tau_{\mathcal{E}} \sim 0.3$ μ s).

This distinct feature is in fact an absolutely crucial element for possible potential observations of the emission. This difference between $\tau_{\mathcal{B}}$ and $\tau_{\mathcal{E}}$ is the main reason for

dramatically different energy injection which is measured in units $\text{MeV} \cdot \text{MHz}^{-1}$ in case of \mathcal{E} -type emission to be contrasted with much lower $\text{keV} \cdot \text{MHz}^{-1}$ scale in case of \mathcal{B} -type emission, see Figs. 3 and 5 correspondingly.

Therefore, the total energy of the radio emission integrated over the pulse time is much greater for the \mathcal{E} -type radiation in comparison with \mathcal{B} -type radiation. Furthermore, the required resolution to detect the very short \mathcal{B} -type pulse with $\tau_{\mathcal{B}} \sim \text{ns}$ requires much more demanding instruments than recording of the conventional \mathcal{E} -type pulses with duration time of order $\tau_{\mathcal{E}} \sim \mu\text{s}$. These arguments strongly suggest that \mathcal{E} -type radiation plays the dominant role in emission processes. Therefore, any future studies (including possible observations) should be focused on \mathcal{E} -type radiation analyzed in Section IV.

VII. CONCLUSION

As we argued at the very end of previous Section VI the \mathcal{E} -type radiation plays the dominant role in radio emission. The corresponding results have been summarized at the very end of Section IV where it has been argued that the radio pulse can be recorded if proper instruments are designed and built at the T ASD site. The pulse must be synchronized with T ASD bursts. Such a signal cannot be confused with any other spurious and noise signals as a result of this synchronization. Therefore, observing (not observing) such synchronized signals can confirm, substantiate or refute our proposal.

Our arguments are entirely based on the AQN framework. Why should we take this model seriously? In section II B we mentioned that this model was originally formulated to resolve simultaneously two fundamental puzzles of the modern cosmology: the observed matter-antimatter asymmetry and the observed similarity between the dark and visible components of the Universe, i.e. the ratio $\Omega_{\text{DM}} \sim \Omega_{\text{visible}}$ holds irrespectively to any specific features of the model.

The basic logic of the construction suggests that there must be many observable consequences of this model. Indeed, the AQNs may offer a resolution [39, 40] to some seemingly unrelated puzzles such as the ‘‘Solar Corona Mystery’’ when the so-called ‘‘nanoflares’’ conjectured by Parker long ago [41] are identified with the annihilation events in the AQN framework. The luminosity of the Extreme UV (EUV) radiation from corona due to these annihilation events is unambiguously determined by the DM density. It is very nontrivial consistency check that the computed luminosity from the corona nicely matches with observed EUV radiation. The same events of annihilation are also manifested themselves as the radio impulsive events [42] in quiet solar corona. The computed intensity and spectral features are consistent with recently recorded radio events in quiet solar corona by Murchison Widefield Array Observatory [43], which also represents a very nontrivial consistency check of the pro-

posal [39, 40] on the ‘‘Solar Corona Mystery’’ resolution.

The AQNs may also offer a resolution of the ‘‘Primordial Lithium Puzzle’’ [44] and the longstanding puzzle with the DAMA/LIBRA observation of the annual modulation at 9.5σ confidence level [45]. Furthermore, it may resolve the observed (by XMM-Newton at 11σ confidence level [46]) puzzling seasonal variation of the X-ray background in the near-Earth environment in the 2-6 keV energy range as suggested in [47]. The AQN annihilation events in the Earth’s atmosphere could produce infrasound and seismic acoustic waves as discussed in [48] when the infrasound and seismic acoustic waves have been recorded without any traces of accompanying meteor-like events. This list of possible observational consequences of the AQN framework is already quite long, but definitely this list is far from being complete.

Our present proposal suggests that the TA bursts with very unusual features will be synchronized with radio pulses. If this synchronization is observed and the interpretation of TA bursts as the AQN annihilation events is confirmed by future studies it would be the *first direct* (non-gravitational) evidence which reveals the nature of the DM, in contrast with large number of *indirect* hints listed above.

ACKNOWLEDGEMENTS

This research was supported in part by the Natural Sciences and Engineering Research Council of Canada, and X.L. also by the UBC four year doctoral fellowship.

-
- [1] R. Abbasi *et al.* (Telescope Array Project), *Phys. Lett. A* **381**, 2565 (2017).
- [2] T. Okuda, *Journal of Physics: Conference Series* **1181**, 012067 (2019).
- [3] A. Zhitnitsky, *J.Phys.G:Nucl.Part.Phys.* (2020), 10.1088/1361-6471/abd457, arXiv:2008.04325 [hep-ph].
- [4] A. R. Zhitnitsky, *JCAP* **10**, 010 (2003), hep-ph/0202161.
- [5] E. Witten, *Phys. Rev. D* **30**, 272 (1984).
- [6] E. Farhi and R. L. Jaffe, *Phys. Rev. D* **30**, 2379 (1984).
- [7] A. De Rújula and S. L. Glashow, *Nature (London)* **312**, 734 (1984).
- [8] J. Madsen, in *Hadrons in Dense Matter and Hadrosynthesis*, Lecture Notes in Physics, Berlin Springer Verlag, Vol. 516, edited by J. Cleymans, H. B. Geyer, and F. G. Scholtz (1999) p. 162, astro-ph/9809032.
- [9] R. D. Peccei and H. R. Quinn, *Phys. Rev. D* **16**, 1791 (1977).
- [10] S. Weinberg, *Phys. Rev. Lett.* **40**, 223 (1978).
- [11] F. Wilczek, *Phys. Rev. Lett.* **40**, 279 (1978).
- [12] J. E. Kim, *Phys. Rev. Lett.* **43**, 103 (1979).
- [13] M. A. Shifman, A. I. Vainshtein, and V. I. Zakharov, *Nucl. Phys. B* **166**, 493 (1980).
- [14] M. Dine, W. Fischler, and M. Srednicki, *Phys. Lett. B* **104**, 199 (1981).
- [15] A. R. Zhitnitsky, *Sov. J. Nucl. Phys.* **31**, 260 (1980), [Yad. Fiz.31,497(1980)].
- [16] K. Van Bibber and L. J. Rosenberg, *Physics Today* **59**, 30 (2006).
- [17] S. J. Asztalos, L. J. Rosenberg, K. van Bibber, P. Sikivie, and K. Zioutas, *Annual Review of Nuclear and Particle Science* **56**, 293 (2006).
- [18] P. Sikivie, in *Axions*, Lecture Notes in Physics, Berlin Springer Verlag, Vol. 741, edited by M. Kuster, G. Raffelt, and B. Beltrán (2008) p. 19, astro-ph/0610440.
- [19] G. G. Raffelt, in *Axions*, Lecture Notes in Physics, Berlin Springer Verlag, Vol. 741, edited by M. Kuster, G. Raffelt, and B. Beltrán (2008) p. 51, hep-ph/0611350.
- [20] P. Sikivie, *International Journal of Modern Physics A* **25**, 554 (2010), arXiv:0909.0949 [hep-ph].
- [21] L. J. Rosenberg, *Proceedings of the National Academy of Science* **112**, 12278 (2015).
- [22] D. J. E. Marsh, *Phys. Rep.* **643**, 1 (2016), arXiv:1510.07633.
- [23] P. W. Graham, I. G. Irastorza, S. K. Lamoreaux, A. Lindner, and K. A. van Bibber, *Annual Review of Nuclear and Particle Science* **65**, 485 (2015), arXiv:1602.00039 [hep-ex].
- [24] I. G. Irastorza and J. Redondo, *Prog. Part. Nucl. Phys.* **102**, 89 (2018), arXiv:1801.08127 [hep-ph].
- [25] X. Liang and A. Zhitnitsky, *Phys. Rev. D* **94**, 083502 (2016), arXiv:1606.00435 [hep-ph].
- [26] S. Ge, X. Liang, and A. Zhitnitsky, *Phys. Rev. D* **96**, 063514 (2017), arXiv:1702.04354 [hep-ph].
- [27] S. Ge, X. Liang, and A. Zhitnitsky, *Phys. Rev. D* **97**, 043008 (2018), arXiv:1711.06271 [hep-ph].
- [28] S. Ge, K. Lawson, and A. Zhitnitsky, *Phys. Rev. D* **99**, 116017 (2019), arXiv:1903.05090 [hep-ph].
- [29] O. Santillán and A. Morano, (2020), arXiv:2011.06747 [hep-ph].
- [30] A. V. Gurevich and K. P. Zybin, *Physics-Uspekhi* **44**, 1119 (2001).
- [31] J. R. Dwyer and M. A. Uman, *Phys. Rep.* **534**, 147 (2014), the Physics of Lightning.
- [32] J. R. Dwyer and L. P. Babich, *Journal of Geophysical Research: Space Physics* **116** (2011), 10.1029/2011JA016494.
- [33] A. V. Gurevich, R. Roussel-Dupre, and G. M. Milikh, *Journal of Geophysical Research: Space Physics* **117** (2012), 10.1029/2011JA017431.
- [34] J. R. Dwyer and L. Babich, *Journal of Geophysical Research: Space Physics* **117** (2012), 10.1029/2011JA017487.
- [35] L. D. Landau and E. M. Lifshitz, *The classical Theory of Fields, 4-th edition* (Butterworth-Heinemann, Oxford, 1975).
- [36] J. D. Jackson, *Classical electrodynamics*, 3rd ed. (Wiley, New York, NY, 1999).
- [37] A. Gurevich, L. Duncan, A. Karashtin, and K. Zybin, *Phys. Lett. A* **312**, 228 (2003).
- [38] J. Schwinger, *Phys. Rev.* **75**, 1912 (1949).
- [39] A. Zhitnitsky, *JCAP* **10**, 050 (2017), arXiv:1707.03400 [astro-ph.SR].

- [40] N. Raza, L. van Waerbeke, and A. Zhitnitsky, *Phys. Rev. D* **98**, 103527 (2018), [arXiv:1805.01897 \[astro-ph.SR\]](#).
- [41] E. N. Parker, *Astrophys. J.* **330**, 474 (1988).
- [42] S. Ge, M. S. R. Siddiqui, L. Van Waerbeke, and A. Zhitnitsky, *Phys. Rev. D* **102**, 123021 (2020), [arXiv:2009.00004 \[astro-ph.HE\]](#).
- [43] S. Mondal, D. Oberoi, and A. Mohan, *Astrophys. J.* **895**, L39 (2020).
- [44] V. V. Flambaum and A. R. Zhitnitsky, *Phys. Rev. D* **99**, 023517 (2019), [arXiv:1811.01965 \[hep-ph\]](#).
- [45] A. Zhitnitsky, *Phys. Rev. D* **101**, 083020 (2020), [arXiv:1909.05320 \[hep-ph\]](#).
- [46] G. W. Fraser, A. M. Read, S. Sembay, J. A. Carter, and E. Schyns, *Mon. Not. Roy. Astron. Soc.* **445**, 2146 (2014), [arXiv:1403.2436 \[astro-ph.HE\]](#).
- [47] S. Ge, H. Rachmat, M. S. R. Siddiqui, L. Van Waerbeke, and A. Zhitnitsky, (2020), [arXiv:2004.00632 \[astro-ph.HE\]](#).
- [48] D. Budker, V. V. Flambaum, and A. Zhitnitsky, (2020), [arXiv:2003.07363 \[hep-ph\]](#).